An Experimental Study on Solitary Waves of a Rotating Disk

Jong-Keun Choi* and Stephen H. Crandall**

(*Received June 6, 1998*)

This paper has been studied on the solitary wave phenomena on the flexible rotating disk by experiment of measuring the separation of solitons. The phenomena have been discovered recently by Crandall and Boulahbal in 1995. They have shown some pictures of solitary waves on a flexible rotating disk by using a high speed camera and fotonic sensor. But there is no theory to explain and predict such solitary waves on a flexible rotating disk with a thin film of fluid. In order to establish this theory and to explain these phenomena, more experiments are needed to describe such waves. This paper attempts to provide such necessary experiments by studying the relations of air inflow gaps, radius of rotating disk and its rotating speed. The separation of solitons has been measured by a fiber optic displacement sensor at each speed. Some conclusions have been obtained from this experiment to describe this new phenomena of solitary waves on a rotating disk. It may be a very qualitative description rather than a quantitative prediction using a mathematical model. However we have measured the separation and taken photographs with a high speed camera; therefore this conclusion could be useful in understanding the phenomena and may contribute to future work.

Key Words: Solitary Waves, Rotating Disk

1. Introduction

A lot of research has been done on the stability and instability of a rotating disk. Those works can be categorized into three classifications. The first class can be categorized by bending rigidity, stiffening effect of rotation, and instability of the rotating disk due to imperfections (Lamb and Southwell (1921), Southwell (1922), Tobias and Arnold (1957)). The second class can be categorized by the effects of the air film, load system, and interactions between the disk and load system (Pelech and Shapiro (1964), Adams (1980), Licari and King (1981), Benson and Bogy (1978), Carpino and Domoto (1988), Hosaka and Nishida (1987), Ono and Maeno (1986), Chen and Bogy (1993), Shen and Mote Jr (1991)). The third class can be categorized by the self excited instability on the vibration of a rotating disk (Hosaka and Crandall (1992), Boulahbal (1995)).

This experimental report is related to the work of Pelech and Shapiro in 1964. They have performed an experiment to describe a flexible disk rotating on a gas film next to a wall. Their pioneering work explored the general rules of behavior which might be inherent in the coupling between the mechanics of a rotating disk and the fluid dynamics of a gas flowing through a gap. They measured the disk's steady state deflection for various conditions of air flow rate and disk radius, but they did not discover the solitary waves on the flexible disk in that experiment.

Solitary wave phenomena on the flexible rotating disk have been discovered recently by Crandall and Boulahbal in 1995. It was not a quantitative measurement of solitons but a taking of pictures of solitary waves and measuring their

* Department of Mechanical Engineering, Kangwon State College, Kangneung, Korea

** Department of Mechanical Engineering, Massachusetts Institute of Technology

frequencies via high speed camera and fotonic sensor. Solitary wave is a highly wrinkled wave on a rotating disk changed from harmonic waves. Figure 1 shows these solitary waves which are moving along the flexible disk with less spin rate than the disk.

We do not have any theory to explain and predict such solitary waves on a flexible rotating disk with a thin film of fluid. In order to establish this theory and to explain these phenomena, more experiments are needed to describe such waves. This paper attempts to provide such necessary experiments. These new observations can not give us quantitative predictions, but instead provide qualitative explanations on how these solitary waves can occur and quantitative displacement measurements for new theory in future. This is the beginning of those works.

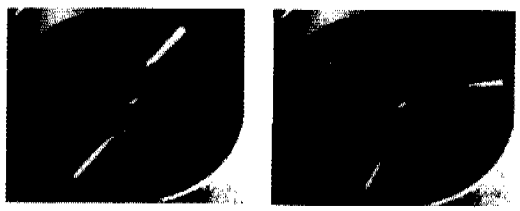

Fig. 1 Solitary waves on the rotating disk: Two and three solitons, 3300rpm, photographs from Boulahbal(1995).

2. Objective

This experiment has been done with two objectives. One is to describe the phenomena of solitons more quantitatively by measuring the separation of the flexible disk from a rigid plate. The other is to provide the experimental data of displacement for proof of a new theoretical model on the phenomena of solitary waves, which occur

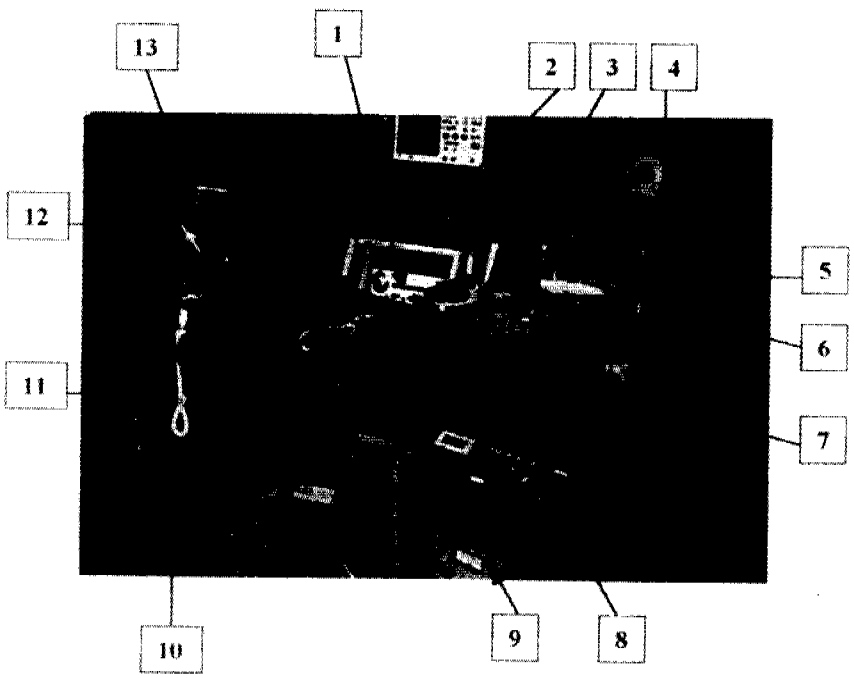

1. Function Generator
2. Data Recorder
3. Strobe Light
4. High Speed Camera
5. Fiber Optic Displacement Sensor Tip
6. Flexible Rotating Disk
7. Amplifier of Fiber Optic Displacement Sensor
8. Control Panel of the Rotating System
9. DC Power Supply
10. Computer for High Speed Camera
11. VCR for High Speed Camera
12. Monitor for High Speed Camera
13. Light for High Speed Camera

Fig. 2 Overview of the experiment instrumentation.

on the flexible disk when it rotates against one rigid plate with high speed.

3. Experimental Apparatus

3.1 Description of the experimental system

Figure 2 shows an overview of the experimental instrumentation, which is composed of the spinning disk system, fiber optic displacement sensor, DC power supply, function generator, data recorder, strobe light and a high speed camera. Figures 3-1 and 3-2 show a few of these.

Figure 4 shows the schematic drawing of the flexible disk rotating system. This system has three different types of speed control; Internal voltage, external voltage and the voltage clock. External voltage control needs a function generator, and it is the best way to get the highest speed among these types. In this experiment, external voltage control has been used. The maximum speed we can get is between 3000 rpm and 4000 rpm, but it is very dependent on its load of rotating disk. This limitation of maximum speed gave us some difficulty for the choice of material of the flexible disk.

Table 1 shows Maker, Model and Specification of the instruments which have been used.

3.2 Fiber optic displacement sensor

A fiber optic displacement sensor has been used to measure the separation between the bottom plate and the flexible rotating disk. The fiber

Fig. 3-1 Fiber optic displacement sensor & amplifier.

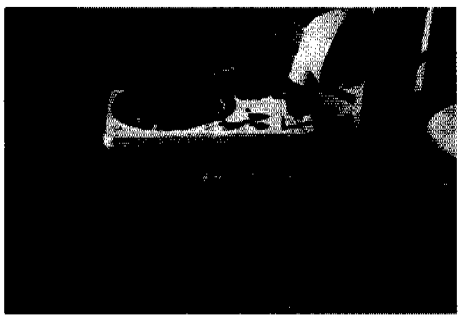

Fig. 3-2 Strobe light.

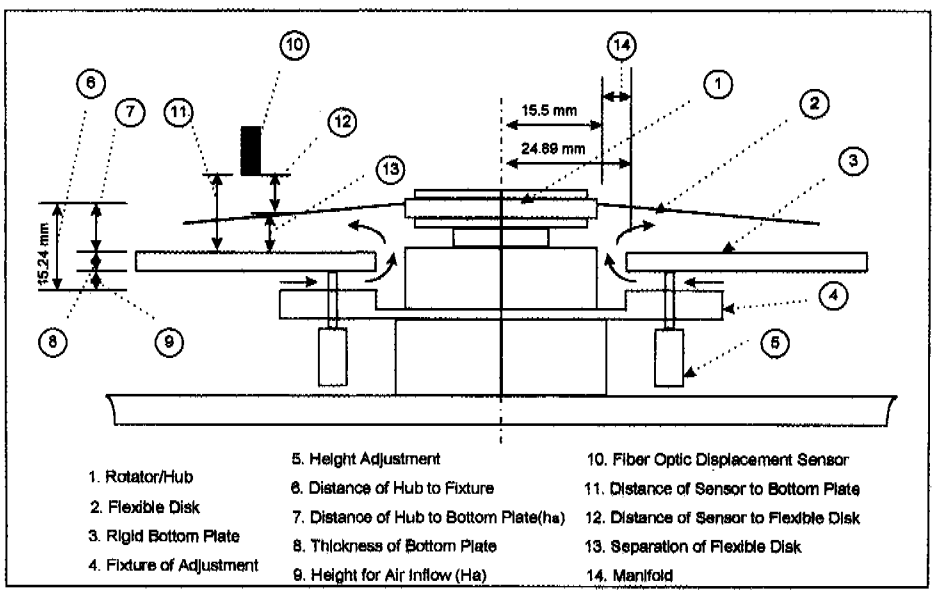

Fig. 4 Schematic drawing of a disk rotating system.

Table 1 Maker & model of instruments.

No	Instrument	Maker	Model	Specification
1	Disk rotating system	NTT & MIT		
2	Fiber optic displacement sensor	PHILTEC	RC 90	0 mm~12.7 mm
3	Functional generator	WAVETEK	187	
4	Data recorder	ONO SOKKI	CF 360	Dual CH FFT
5	Strobe light	General radio	1538-A	150000 rpm
6	DC power supply	Hewlett packard	6286A	0-20V
7	High speed camera	KODAK	Ektapro	1000 Frames/s

optic displacement sensor which has been used in this experiment has an overall range of 12.7 mm (500 mils), and a resolution of 20kHz. Since this sensor has a built-in amplifier, it rarely has noise signals in its data. In order to get a data over the linear range we have used the fifth order polynomial fit which the maker has suggested.

3.3 Flexible disk

The MIT/HAVARD COOP plastic bag of 0. 0508 mm(0. 002 in) thickness has been used for the flexible rotating disk in this experiment. We wanted to change the thickness and tried to use Mylar with thickness of 0.0254 mm, 0.0508 mm and 0.0762 mm, which was specially ordered from the maker. But it had too much static electricity and stuck to the rigid plate, and therefore the rotating torque of the motor could not overcome it. It also wrinkled after a single run; Mylar was therefore not a suitable material for this experiment. A plastic shopping bag was reported by Boulahbal(1995) as a suitable material for this experiment, so we chose this option.

To obtain the material properties for this plastic bag, we cut out circular shapes with a radius of 50mm, 70mm and 100mm. We measured the mass of these by using 4 decimal balance to do it as accurately as possible. We then calculated the density by dividing the mass by its volume. To get the Young's Modulus we measured the deflection in cantilever and calculated the Young's Modulus by the beam theory. We understand this material is non-isotropic and it is very difficult to get the exact material property with this simple test. Even if this value could not be the exact material property, it could be a guide with some error. To measure more accurately, the help of a material test scientist would be required. Density and Young's Modulus of this plastic bag from above test are 946. 54 kg/m^3 and 3. 47E+08 N/m^2.

4. Measurement

To understand what makes the solitary waves we have tried three different air inflow gaps at each of three different radii of flexible disks. Data in three different RPMs and 5 to 9 points on the disk in radial direction have been acquired at each air inflow gap stage. The reason we have taken three different air inflow gaps was that we recognized from the preliminary test that the solitary waves were much more affected from these air inflow gaps shown in Figure 4, which represented schematic drawing of flexible disk rotating system. In Fig. 4, element 6 means a fixed distance of hub to the fixture, which is 15.24 mm. The element 8 means a thickness of the bottom plate, which is 3.175 mm. The element 7 means the distance from the hub to the bottom plate(h_a), which is related to the element 9, height for air inflow(H_a). The height of this air inflow(H_a) has been varied, and the effect has been examined as shown in Table 2. Therefore the plot on hub shown in Fig. 14 to Fig. 40 represents the distance from the hub to the bottom plate(h_a), h_a = element 6-thickness of bottom plate-H_a. The element 14 means a manifold that the air flows out, which is also represented in Fig. 14 to Fig. 40.

Table 2 Classification of measurements.

R (Radius of Disk)	Ha (Air Inflow Gap)	RPM	r/R
101.6 mm (4 in)	2.48 mm	3 steps	5 points
127 mm (5 in)	5.71 mm	3 steps	7 points
152 mm (6 in)	8.94 mm	3 steps	9 points

The distance from the sensor to the bottom plate has been fixed by using a fixture in Fig. 3-1 at each air inflow gap, and the distance from the sensor to the flexible disk has been measured. Then we calculated the separation of flexible disk from the bottom plate ; element 13 = element 11 - element 12 in Fig. 4. The separation of the vertical axis in Fig. 5 to Fig. 40 represent this.

The photographs have also been taken by using a high speed camera and recorded on video tape for each case. But the measurement of displacements and the recording on video tape using a high speed camera were not performed simultaneously, due to technical reasons. Table 2 shows the classification of measurements.

5. Results of Measurements

There are so many graphs on the time domain at each radius of disk as shown in Table 3 that we have extracted some typical ones to illustrate solitary waves, transient waves and harmonic waves.

Figures 5 to 13 represent these typical graphs

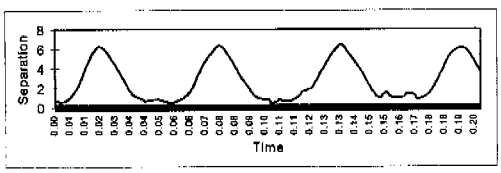

Fig. 5 Separation of 4 solitons at R=101.6 mm, Ha=2.48 mm, rpm=1219, r/R=0.625

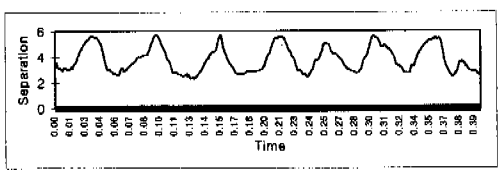

Fig. 6 Separation of 4 solitons at R=101.6 mm, Ha=5.71 mm, rpm=1322, r/R=0.625

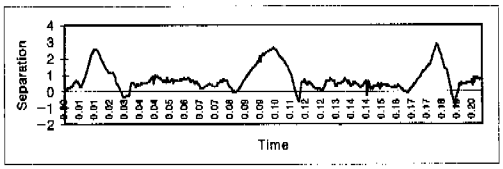

Fig. 7 Separation of 2 solitons at R=101.6 mm, Ha=8.94 mm, rpm=1176, r/R=0.625

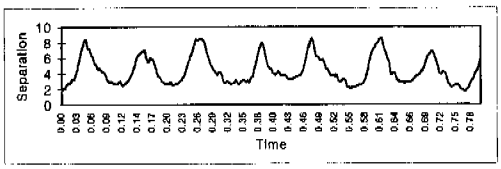

Fig. 8 Separation of 2 solitons at R=127 mm, Ha=2.48 mm, rpm=625, r/R=0.4

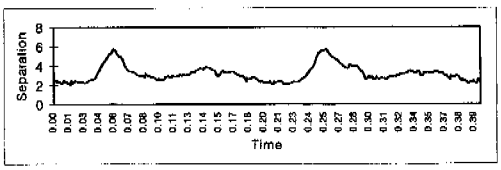

Fig. 9 Separation of 2 solitons at R=127 mm, Ha=5.71 mm, rpm=630, r/R=0.4

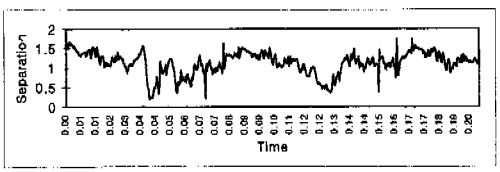

Fig. 10 Separation for transition of soliton at R=127mm, Ha=8.94 mm, rpm=718, r/R=0.4

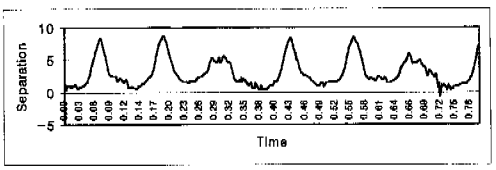

Fig. 11 Separation of 3 solitons at R=152 mm, Ha=2.48 mm, rpm=603, r/R=0.4

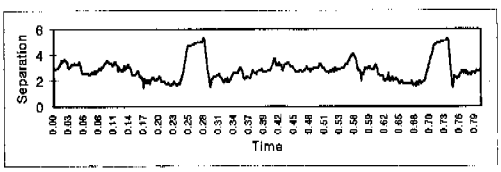

Fig. 12 Separation of 2 solitons at R=152 mm, Ha=5.71 mm, rpm=602, r/R=0.4

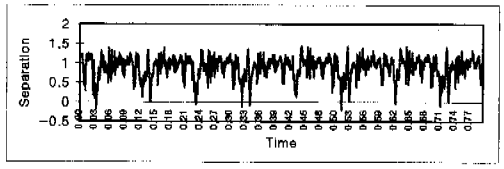

Fig. 13 Separation of no solitons at R=152 mm, Ha=8.94 mm, rpm=611, r/R=0. 4

on time domain. The number of solitons in Fig. 5 ~13 are counted by a strobe light, which might have a little different result than with using a high speed camera. When using the strobe light we have to fit the frequency of the strobe light to the speed of the solitary wave. Then the moving shape of the solitary wave can be fixed and we can recognize the number of solitons and its speed. Since it may be a little bit subjective and not easy to fit exactly, using a high speed camera is better for counting the number of solitons. Once getting the exact number of solitons whatever we use, the periodic speed of solitons can be calculated exactly by the data on the time domain. If the periodic shape of solitons of data on the time domain is obvious as shown in Fig. 11, and it shows a good match with the number counted by the strobe light, then the periodic speed of solitons can be calculated without a high speed camera. The frequency of soliton in Fig. 11 is 2. 73 and its rpm is 164. The speed of the disk is 3. 67 times higher than the speed of solitary waves in this case. The number of solitons described in Fig. 5 to Fig. 13 are from using the strobe light.

Since the number of solitons is very dependent on the initial condition as reported by Boulahbal (1995), counting the number is less important than describing the displacement of solitons at this stage. To get the number and speed of solitons more accurately we have to use the high speed camera and fiber optic displacement sensor simultaneously. We have not done this in this experiment as aforementioned.

Figures 7, 10 and 13 show changes of solitons, as well as the transient zone and the harmonic behavior with a variation of the radius of a disk at the same gap of air inflow. It suggests that the bigger a radius of disk becomes, the greater the possibility of disappearance of solitons would be.

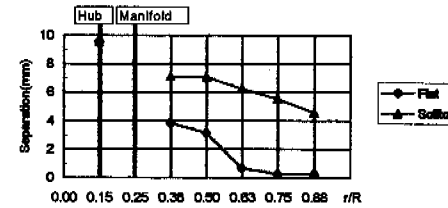

Fig. 14 Separation at R=101.6 mm, Ha=2.48 mm, rpm=1219

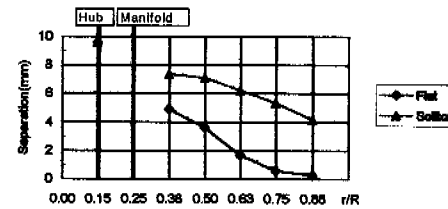

Fig. 15 Separation at R=101.6 mm, Ha=2.48 mm, rpm=2049

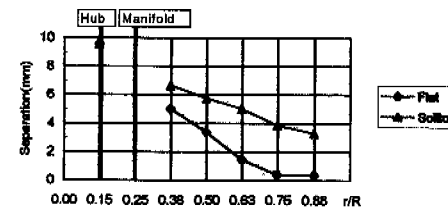

Fig. 16 Separation at R=101.6 mm, Ha=2.48 mm, rpm=3607

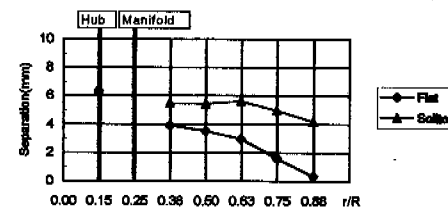

Fig. 17 Separation at R=101.6 mm, Ha=5.71 mm, rpm=1322

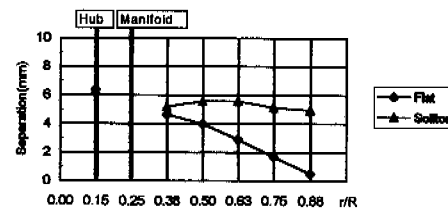

Fig. 18 Separation at R=101.6 mm, Ha=5.71 mm, rpm=2486

Figures 11, 12 and 13 show changes in disappearance of solitons with a variation of the air

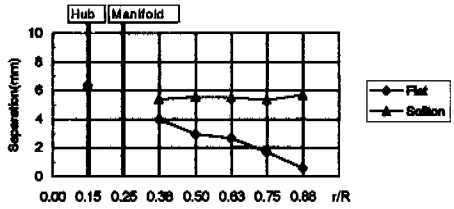

Fig. 19 Separation at R=101.6 mm, Ha=5.71 mm, rpm=3596

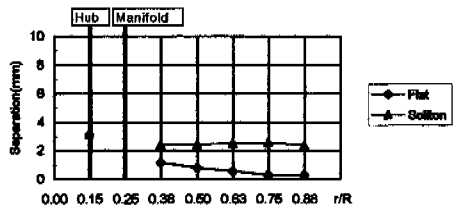

Fig. 20 Separation at R=101.6 mm, Ha=8.94 mm, rpm=1176

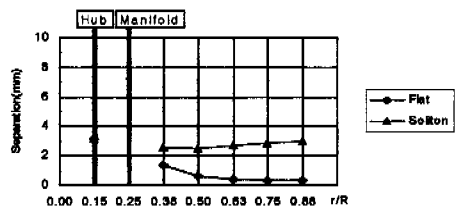

Fig. 21 Separation at R=101.6 mm, Ha=8.94 mm, rpm=2307

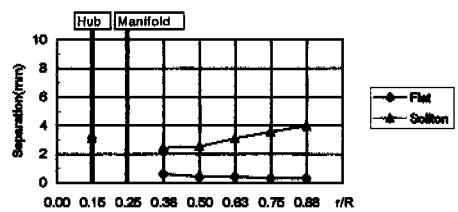

Fig. 22 Separation at R=101.6 mm, Ha=8.94 mm, rpm=3336

inflow gap at the same radius and similar rpm. It suggests the smaller the air inflow gap becomes, the easier solitons occur and vise versa. This implies the air flow rate between a rigid wall and flexible rotating disk is a very important factor in making solitons.

Figures 14 to 40 show the separation of flexible disks from a rigid plate with a variation of the radius of the flexible disk, air inflow gap and rpm at each of three different stages.

Figures 14 to 22 represent the case of the smallest radius, R=101.6 mm. It shows solitons in all the stages of Ha and RPM, where Ha means the air inflow gap. Figures 17 to 19 represent the middle of Ha at increasing RPM. It shows the

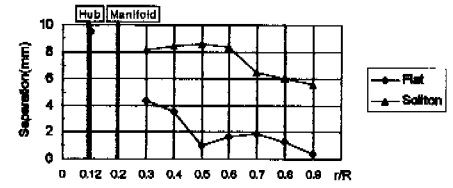

Fig. 23 Separation at R=127 mm, Ha=2.48 mm, rpm=625

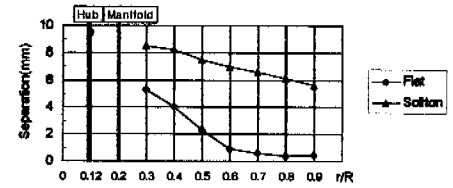

Fig. 24 Separation at R=127 mm, Ha=2.48 mm, rpm=1249

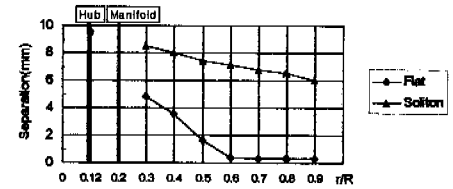

Fig. 25 Separation at R=127 mm, Ha=2.48 mm, rpm=1904

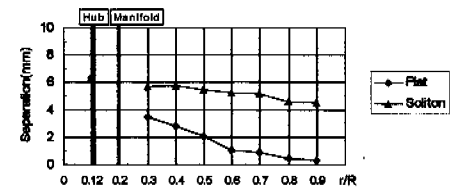

Fig. 26 Separation at R=127 mm, Ha=5.71 mm, rpm=630

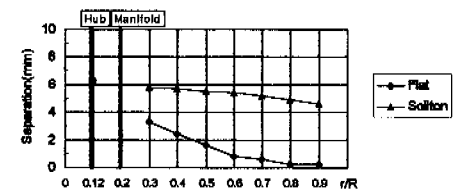

Fig. 27 Separation at R=127 mm, Ha=5.71 mm, rpm=1206

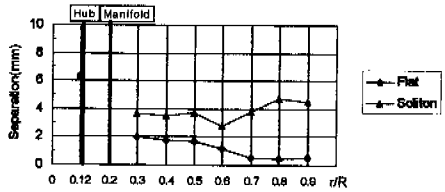

Fig. 28 Separation at R=127 mm, Ha=5.71 mm, rpm=2540

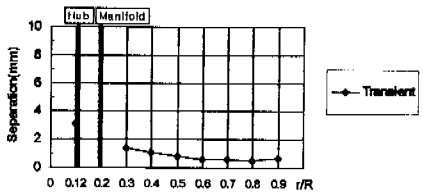

Fig. 29 Separation at R=127 mm, Ha=8.94 mm, rpm=718

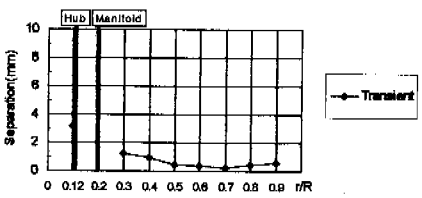

Fig. 30 Separation at R=127 mm, Ha=8.94 mm, rpm=2929

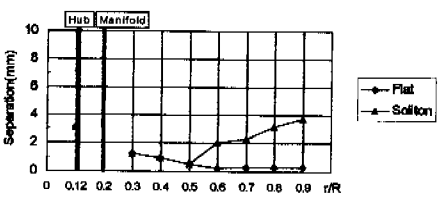

Fig. 31 Separation at R=127 mm, Ha=8.94 mm, rpm=3788

outer edge of solitons are going higher with speed. Figures 20 to 22 represent the highest Ha, it means the smallest distance from the hub to the bottom plate as shown in Fig. 4. It shows the outer soliton edge of the disk is higher than the edge of the hub.

Figures 23 to 31 represent the case of the middle radius, R=127 mm. In the highest Ha of the middle radius it shows no solitons in low RPM. Figures 29 and 30 represent this phenomena. Figure 29 is related to Fig. 10, which is a data on the time domain. It represents a transient

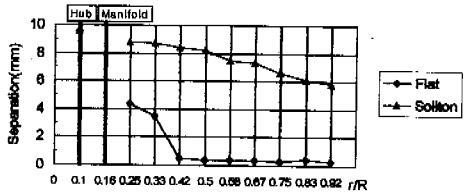

Fig. 32 Separation at R=152 mm, Ha=2.48 mm, rpm=603

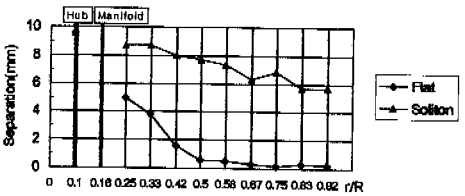

Fig. 33 Separation at R=152 mm, Ha=2.48 mm, rpm=1201

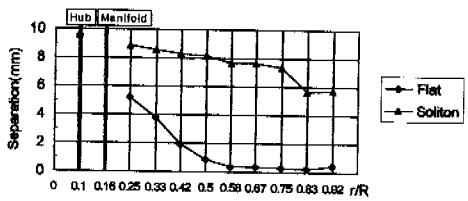

Fig. 34 Separation at R=152 mm, Ha=2.48 mm, rpm=1801

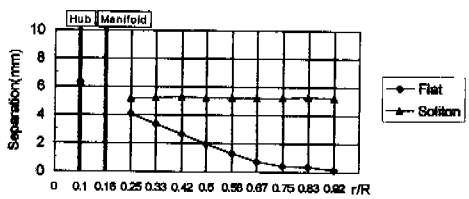

Fig. 35 Separation at R=152 mm, Ha=5.71 mm, rpm=602

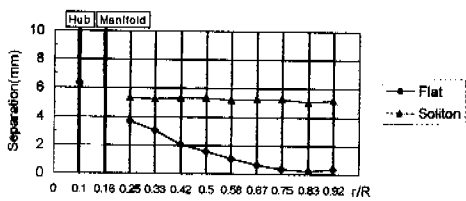

Fig. 36 Separation at R=152 mm, Ha=5.71 mm, rpm=1208

phonomenon. Figure 30 also shows a transient from data using a fiber optic sensor, but when we took a look at the video tape using a high speed

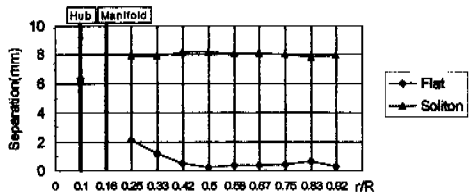

Fig. 37 Separation at R=152 mm, Ha=5.71 mm, rpm=1793

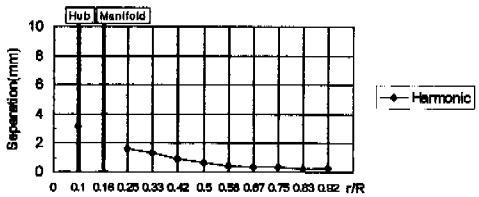

Fig. 38 Separation at R=152 mm, Ha=8.94 mm, rpm=611

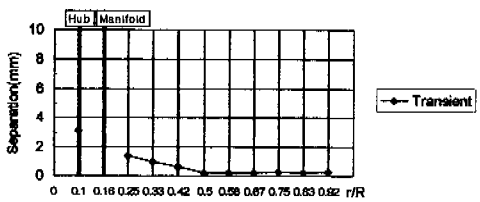

Fig. 39 Separation at R=152 mm, Ha=8.94 mm, rpm=2350

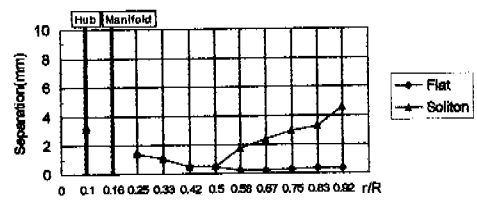

Fig. 40 Separation at R=152 mm, Ha=8.94 mm, rpm=2922

camera, it showed five or six very small solitons on the edge of the disk. Because we did not take both the fiber optic sensor and the video tape recording simultaneously, some difference might have occurred in this case due to its initial condition. Figure 31 shows the soliton edge of the disk is higher than the edge of the hub as Fig. 22 shows.

Figures 32 to 40 represent the case of the biggest radius, R=152 mm. Figure 38 is related to Fig. 13 of data on time domain. It shows no solitons but a harmonic motion, and a good match with the video tape taken with a high speed camera. Figure 39 shows a transient area between the harmonic and the solitary waves. It showed many small waves look like solitons on the edge of the disk when we took a look at the video. Figure 40 shows eight small solitons on the video tape. Even though we did not describe this in the report as a form of separation data, when we increased its RPM to 3065 it showed four big solitons on the video tape, which was reduced from eight small solitons in Fig. 40. When we touched the disk slightly its number of solitons reduced to three. These changes were recorded on the video tape. As shown in Fig. 40, the soliton edge of the disk is going higher than the edge of the hub as in Fig. 22 and Fig. 31.

6. Conclusion

We now have five conclusions from this experiment to describe this new phenomena of solitary waves on a rotating disk. It may be a very qualitative description rather than a quantitative prediction using a mathematical model. However the separation has been measured and the photographs have been taken with a high speed camera; therefore this conclusion could be useful in understanding the phenomena and may contribute to future work.

(1) There exists a transient zone between the harmonic motion and the solitary wave motion.

(2) The smaller a radius of a rotating disk becomes, the more easily solitary waves can occur at the same condition.

(3) The air inflow gap and the initial air outflow gap(the distance between the hub and bottom plate) are much more important factors in making solitary waves than the radius of the disk. The critical speed has been changed for the variation in the air inflow gap, but it has not been changed for the variation of the radius.

(4) The higher a rotational speed gets, the higher the separation for the soliton edge of the disk becomes from the edge of the hub.

(5) The number of solitons is very dependent on the initial condition and some perturbation

during running, therefore it is very difficult to predict this number before the running.

Reference

Adams, G. G., 1980, "Analysis of the Flexible Disk/Head Interface," *Transactions of the ASME, Journal of Lubrication Technology*, 102, pp. 86~90.

Benson, R. C. and Bogy, D. B., 1978, "Deflection of a Very Flexible Spinning Disk due to a Stationary Transverse Load," *Transactions of the ASME, Journal of Applied Mechanics*, 45, pp. 636~642.

Boulahbal, D., 1995, *Self-Excited Vibrations of a Spinning Disk*, Doctoral thesis, MIT.

Carpino, M. and Domoto, G. A., 1988, "Investigation of a Flexible Disk Rotating near a Rigid Surface," *Transactions of the ASME, Journal of Tribology*, 110, pp. 664~669.

Chen, J. and Bogy, D. B., 1993, Natural Frequencies and Stability of a Flexible Spinning Disk-Stationary Load System with Rigid Body Tilting," *Transactions of the ASME, Journal of Applied Mechanics*, 60, pp. 470~477.

Hosaka, H. and Crandall, S. H., 1992, "Self-Excited Vibrations of a Flexible Disk Rotating on an Air-Film above a Flat Surface, *ACTA Mechanica (Suppl.)*, 3, pp. 115~127.

Hosaka, H. and Nishida, Y., 1987, "An Elastic Analysis of Back-Plate-Type Foil Disks," *ASLE*, SP-22, pp. 167~173.

Lamb, H. and Southwell, R. V., 1921, "The Vibrations of a Spinning Disc," *Proceedings of the Royal Society*, pp. 272~280.

Licari, J. P. and King, F. K., 1981, "Elastohydrodynamic Analysis of Head to Flexible Disk Interface Phenomena," *Transactions of the ASME, Journal of Applied Mechanics*, 48, pp. 763~768.

Ono, K. and Maeno, T. 1986, "Theoretical and Experimental Investigation on Dynamic Characteristics of a 3.5 inch Flexible Disk due to a Point Contact Head," *ASLE*, SP-21, pp. 144~151.

Pelech, I. and Shapiro, A. H., 1964, "Flexible Disk Rotating on a Gas Film Next to a Wall," *Transactions of the ASME, Journal of Applied Mechanics*, pp. 577~584.

Shen, I. Y. and Mote Jr, C. D., 1991, "On the Mechanisms of Instability of a Circular Plate under a Rotating Spring-Mass-Dashpot System," *Journal of Sound and Vibration*, 148(2), pp. 307~318.

Southwell, R. V., 1922, "On the Free Transverse Vibration of a Uniform Disc Clamped at its Centre; and on the Effects of Rotation," *Proceedings of the Royal Society*, 101, pp. 133~153.

Tobias, S. A. and Arnold, R. N., 1957, "The Influence of Dynamical Imperfection on the Vibration of Rotating Disks," *Proceedings of the Institution of Mechanical Engineers*, 171, pp. 669~690.